ADVANCES IN ATMOSPHERIC SCIENCES, VOL. 30, NO. 1, 2013, 167–174

Intensified Eastward and Northward Propagation of Tropical Intraseasonal Oscillation over the Equatorial Indian Ocean in a Global Warming Scenario

YANG Jing[1] (杨 静), BAO Qing*[2] (包 庆), and WANG Xiaocong[2] (王晓聪)

[1]*State Key Laboratory of Earth Surface Processes and Resource Ecology, Beijing Normal University, Beijing* 100875

[2]*State Key Laboratory of Numerical Modeling for Atmospheric Sciences and Geophysical Fluid Dynamics, Institute of Atmospheric Physics, Chinese Academy of Sciences, Beijing* 100029

(Received 13 December 2011; revised 22 March 2012)

ABSTRACT

Northward propagation in summer and eastward propagation in winter are two distinguished features of tropical intraseasonal oscillation (TISO) over the equatorial Indian Ocean. According to numerical modeling results, under a global warming scenario, both propagations were intensified. The enhanced northward propagation in summer can be attributed to the enhanced atmosphere–ocean interaction and the strengthened mean southerly wind; and the intensified eastward propagation in winter is associated with the enhanced convection-wind coupling process and the strengthened equatorial Kevin wave. Future changes of TISO propagations need to be explored in more climate models.

Key words: northward propagation, eastward propagation, tropical intraseasonal oscillation, global warming

Citation: Yang, J., Q. Bao, and X. C. Wang, 2013: Intensified eastward and northward propagation of tropical intraseasonal oscillation over the equatorial Indian Ocean in a global warming scenario. *Adv. Atmos. Sci.*, **30**(1), 167–174, doi: 10.1007/s00376-012-1260-3.

1. Introduction

Tropical intraseasonal oscillation (TISO) is one of the most significant signals in the tropical atmosphere. The most dominant component of TISO during boreal winter is Madden-Julian Oscillation (MJO) (Madden and Julian, 1971, 1972), characterized by eastward propagation trapped along the equator (Madden and Julian, 1994; Zhang, 2005). Eastward-propagating MJO plays a significant role in the weather and climate systems during boreal winter, including regional droughts (Joseph et al., 2008) and floods (Bond and Vecchi, 2003; Jones et al., 2004), triggering or terminating some El Niño events (Takayabu et al., 1999; Kessler and Kleeman, 2000; Bergman et al., 2001), modulating the biological and chemical components in the atmosphere (Waliser et al., 2005; Tian et al., 2008), and influencing the extra-tropics by driving teleconnections (Liebmann and Hartmann, 1984; Pan and Li, 2008).

Whereas the strong eastward-propagating TISO (the MJO mode) is primarily observed in boreal winter, the TISO in boreal summer (also called as boreal summer ISO: BSISO) is dominated by northward propagation from the equatorial zone to the South Asian monsoon region (e.g., Yasunari, 1979; Krishnamurti and Subrahmanyam, 1982; Wang and Rui, 1990; Yang et al., 2008). The fluctuation of this mode is initiated by eastward-propagating disturbances developing over the equatorial Indian Ocean and is associated with major "active" (wet) and "break" (dry) cycles of the Indian monsoon (Annamalai and Slingo, 2001; Rajeevan et al., 2010). Therefore, the northward-propagating mode of BSISO is closely associated with

*Corresponding author: BAO Qing, baoqing@mail.iap.ac.cn.

the occurrences of droughts and floods over the South Asian summer monsoon region (e.g., Ding and Wang, 2009).

Therefore, how the eastward and northward propagations change in the future is very crucial to regional climate and weather changes over the Indian Ocean, the Maritime Continent, and the South Asian monsoon region. Because global climate models still do not realistically reproduce all characteristics of the TISO (e.g., Zhang, 2005; Lin et al., 2006; Kim et al., 2009), the question of how global warming will further impact the MJO has not been widely explored. A recent study has investigated the modification of MJO activity by global warming using a stochastic model; investigators focused on the mean number of MJO events and the probability of MJO active years (Jones and Carvalho, 2011). Both significantly increased. However, the changes in eastward and northward propagations under global warming have not been investigated.

In preparation for the coordinated numerical experiments under the Intergovernmental Panel on Climate Change (IPCC) Fifth Assessment Report (AR5) (http://www.ipcc.ch/activities/activities.shtml), the Institute of Atmospheric Physics, Chinese Academy of Sciences (IAP) coupled model FGOALS-s (the Flexible Global Ocean–Atmosphere–Land System model) was used to conduct both historical simulations and extended simulations of different climate-change scenarios (Bao et al., 2010). Based on the output data from these simulations, Yang et al. (2011) comprehensively evaluated the performances of TISO simulations in atmospheric-only and atmosphere–ocean coupling simulations, respectively, and found that the coupled model better captured TISO features. In this study, we investigated the changes in TISO propagation in a future global warming scenario using the coupled model. We further analyzed the possible causes of the changes demonstrated by our results.

2. Model and experimental design

2.1 *IAP FGOALS model*

The climate-system model used in this study was the second spectral version of FGOALS2-s, developed by the State Key Laboratory of Numerical Modeling for Atmospheric Sciences and Geophysical Fluid Dynamics (LASG) at IAP. This model has provided recent state-of-the-art climatological simulations of the Earth's past, present, and future climate states (Bao et al., 2010). The atmospheric component of this model is the spectral atmospheric model of the IAP/LASG (SAMIL) (Wu et al., 1996; Bao et al., 2010), and its horizontal resolution is 2.81° (lon.)×1.66° (lat.) with 26 hybrid vertical layers. The oceanic component is LASG IAP Common Ocean Model (LICOM) (Liu et al., 2004), and its grid resolution is 1°×1° with increased resolution to 0.5°×0.5° in tropical regions. The other components, including land surface, ice, and coupler components were obtained from the NCAR CCSM (Community Earth System Model) (Kiehl and Gent, 2004).

2.2 *The IPCC AR5 scenarios*

To investigate the projected changes of TISO propagation, three groups of CMIP5 (Coupled Model Intercomparison Project Phase 5) (http://cmip-pcmdi.llnl.gov/cmip5/) coordinated experiments with FGOALS2-s were used: historical simulations and representative concentration pathways (RCP; http://www.iiasa.ac.at/Research/ENE/IAMC/rcp.html) at future projection levels of 4.5 and 8.5. The historical simulations were integrated from 1850 to 2005. The results of the 11-year integration from 1991 to 2001 were used to depict the current situations. Both RCP simulations were projected from 2006 to 2100, where the 4.5 level denotes an RCP with radiative forcing of ∼4.5 W m^{-2} at year 2100, relative to preindustrial conditions (year 1850) (Taylor et al., 2009). Likewise, the 8.5 level denotes an RCP with radiative forcing of ∼8.5 W m^{-2} at year 2100. We named the global warming simulations in this study RCP4.5 and RCP8.5. RCP4.5 is a stabilization scenario in which total radiative forcing is stabilized before 2100, which can be achieved utilizing a range of new technologies and strategies for reducing greenhouse gas emissions. RCP8.5 represents unmitigated increasing greenhouse gas emissions over time, resulting in high greenhouse gas concentration levels. The results of an 11-year integration from 2090 to 2100 represent the global warming scenario; they were used to facilitate the comparison with the current situation. Although the results of both RCP8.5 and RCP4.5 were clear, the signals were more obvious in RCP8.5, so our analysis was based on the RCP8.5 result. The mean sea surface temperatures in both the historical simulation (CTL) and RCP8.5 are shown in Fig. 1.

The changes imposed in historical simulations and future projections included atmospheric composition (including CO_2), due to anthropogenic and volcanic influences, solar forcing, and concentrations of short-lived species and natural and anthropogenic aerosols. These experiments were all standard simulations based on CMIP5 experimental design (Taylor et al., 2009; Moss et al., 2010).

3. Data and methodology

The observation datasets included the daily and

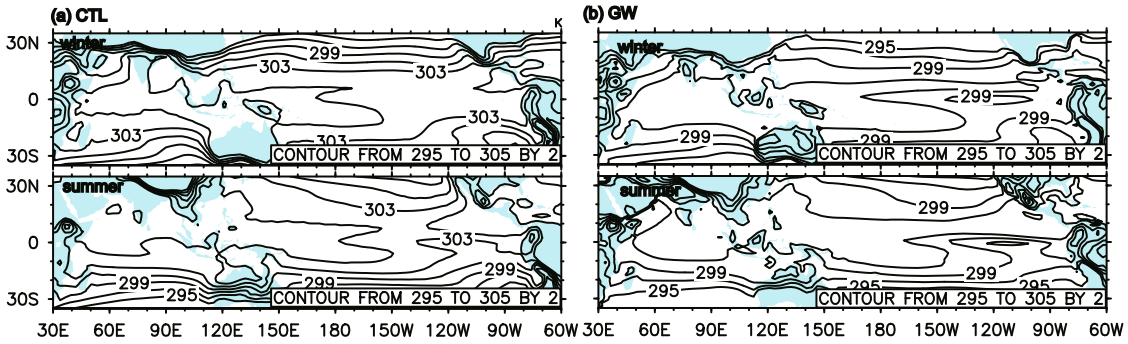

Fig. 1. Sea surface temperature (SST) distribution during winter (Nov.–Apr.) and summer (Mar.–Oct.) respectively in (a) historical control simulation and (b) global warming simulation; units: K.

monthly rainfall data from the Global Precipitation Climatology Project (GPCP, Huffman et al., 2001), the daily and monthly wind data from NCEP/NCAR reanalysis (Kalnay et al., 1996), the daily sea surface temperature (SST) from the Tropical Rainfall Measuring Mission (TRMM) microwave imager (TMI) (Wentz et al., 2000), and the SST monthly mean data from the Hadley Center (Rayner et al., 2003). Considering the availability of records from these datasets, the observation period 1998–2007 was selected for comparison with the 11-year model simulation in both historical (CTL) and global warming (RCP8.5) simulations.

The Climate Variability and Predictability World Climate Research Program (CLIVAR) established the Madden-Julian Oscillation Working Group (MJOWG), which developed a standardized set of diagnostics to evaluate MJO simulation in climate models (CLIVAR MJOWG 2008, http://www.usclivar.org/mjo.php). These methodologies have been introduced in detail by Waliser et al. (2009) and Kim et al. (2009). In this study, we applied these diagnostics to evaluate the propagation and other activities of TISO/MJO. The boreal winter was defined as November to April (November–April), and the boreal summer was defined as May to October (May–October). The 20–100-day bandpass-filtered anomalies were constructed using a 201-point Lanczos filter (Duchon, 1979) with half-power points at 20- and 100-day intervals.

4. Results and discussion

4.1 *Change of northward propagation during boreal summer*

Based on the MJOWG diagnostic package, northward propagation of the TISO was modeled using a lagged-time–latitude diagram of correlation coefficients between 20–100-day bandpass-filtered precipitation (Fig. 2, color shadings) and 850 hPa zonal wind (Fig. 2, contours) over 75°–100°E during boreal summer against to the 20–100-day bandpass-filtered pre-

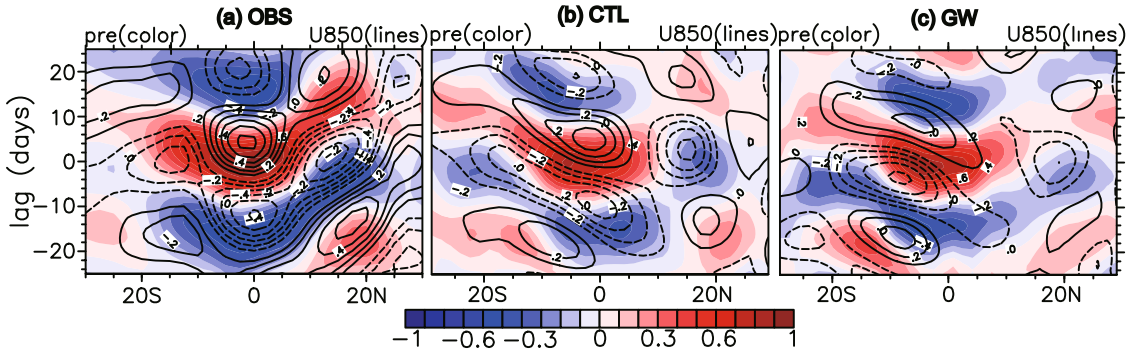

Fig. 2. Lagged-time–latitude diagram of correlation coefficients between 20–100- day band-pass filtered precipitation (color shadings) and U850 (contours) over 75°–100°E during boreal summer against to the 20–100-day filtered precipitation over the reference region (5°N–10°S and 75°–100°E), respectively for (a) observation, (b) CTL, and (c) GW simulations. Contours and color shadings are plotted every 0.1. Contour interval is 0.1.

cipitation over the equatorial Indian Ocean reference region (5°N–10°S and 75°–100°E) (i.e., the IO reference domain) in the TISO component during boreal summer (Fig. 2). According to observations, TISO propagates northward from the equator to around 25°N over the South Asian monsoon region (Fig. 2a). In CTL, the northward propagation was very weak in precipitation and disappeared in U850 (Fig. 2b). The bias of northward propagation in historical simulations has been discussed in a recent work (Yang et al., 2011); it might be associated with the mean state errors of precipitation and SST over the Indian Ocean. Then, what could happen under global warming situation? The result shows that the northward propagation is evidently enhanced under RCP8.5 compared with our historical simulation, CTL, especially in precipitation, particularly between 5°N and 15°N (Fig. 2c).

To investigate the intensification of northward propagation of TISO over the Indian Ocean under global warming, we examined the possible factors influencing the northward propagation of TISO. Previous studies have shown that atmosphere–ocean coupling (e.g., Wang and Xie, 1998; Waliser et al., 1999; Fu and Wang, 2004) can enhance northward propagation of TISO over the Indian Ocean. Figure 3a shows that the quadrature phase relationship between the filtered SST and precipitation data (Waliser et al., 1999; Matthews, 2000) is more obvious between 5°N and 15°N in RCP8.5 than in CTL, which indicates that the atmosphere–ocean coupling processes intensified as a result of global warming. The atmosphere–ocean interaction resulted in positive SST anomalies that enhanced the initial low-level convergence and caused deep convection. Correspondingly, we examined the divergence–precipitation relationship. The quadrature phase relationship between 925-hPa divergence and precipitation in the latitudes of 5°–15°N also appeared in the RCP8.5 simulation (Fig. 3b). Therefore, the strengthened atmosphere–ocean interaction can be considered to be one factor that enhances the northward propagation of TISO during boreal summer.

Additionally, two major internal atmospheric dynamics mechanisms have been proposed by Jiang et al. (2004) to explain northward propagation of TISO over the Indian Ocean. The first is the presence of vertical shear in the mean flow, which can directly generate barotropic vorticity and cause moisture convergence in the planetary boundary layer (PBL), leading to a northward shift of the convective heating that induces northward propagation of TISO. The second is the moisture–convection feedback mechanism, which is associated with two processes: (1) the moisture advection by the mean southerly in the PBL, and (2) the moisture advection by TISO wind due to the mean meridional specific humidity gradient. Accordingly, we examined the changes of the associated three mean states: vertical shear, mean meridional wind, and specific humidity gradient. Our results show that the changes of both vertical shear and specific humidity gradient could not have caused the enhanced northward propagation of TISO according to the theoretical framework of Jiang et al. (2004) (figures not shown here).

Evidently, the lower-level southerly wind over the Indian Ocean significantly strengthened, particularly between the equator and 20°N in RCP8.5 (Fig. 3c), which could have enhanced the northward propagation of moisture. According to Jiang et al. (2004), a strong TISO convection has a convergence at the surface and a divergence at upper levels. The convergence at the surface induces the upward motion and brings rich moisture from the surface to a certain level in the PBL. The advection effect by the summer mean southerly wind in the PBL may have shifted the specific humidity center to the north of the convection which led to the northward displacement of the convection. Therefore, the strengthened southerly mean flow in RCP8.5 enhanced this effect and intensified the northward propagation of TISO.

4.2 *Change of eastward propagation*

Following the MJOWG diagnostic matrix, the eastward propagation of the MJO occurred through lagged-time–longitude diagram of correlation coefficients between 20–100-day filtered precipitation and U850 along the equator (10°N–10°S) on the 20–100-day filtered precipitation over the Indian Ocean during boreal winter (Fig. 4). According to observation data (Fig. 4a), the signal of MJO rainfall propagated eastward from the Indian Ocean to western Pacific Ocean (WP), with an averaged speed of 5 m s^{-1}, and vanished in the eastern Pacific (e.g., Weickmann et al., 1985). Its signal in wind continued to propagate farther east as free (uncoupled with convection) waves at much higher speeds of ∼30–35 m s^{-1} (e.g., Milliff and Madden, 1996; Matthews, 2000). In convectively coupled propagation, precipitation and U850 tended to occur in quadrature, with the maximum in precipitation surpassing that in 850-hPa westerly wind, which is a classic MJO structure (described first by Madden and Julian, 1972).

In the CTL simulation (Fig. 4b), the eastward propagation vanished in both wind and rainfall over the Indian Ocean. The eastward propagation in precipitation occurred over the western Pacific but was very weak. The eastward propagation in wind was evident from the western Pacific to the central Pacific, but it was much weaker than observations. In

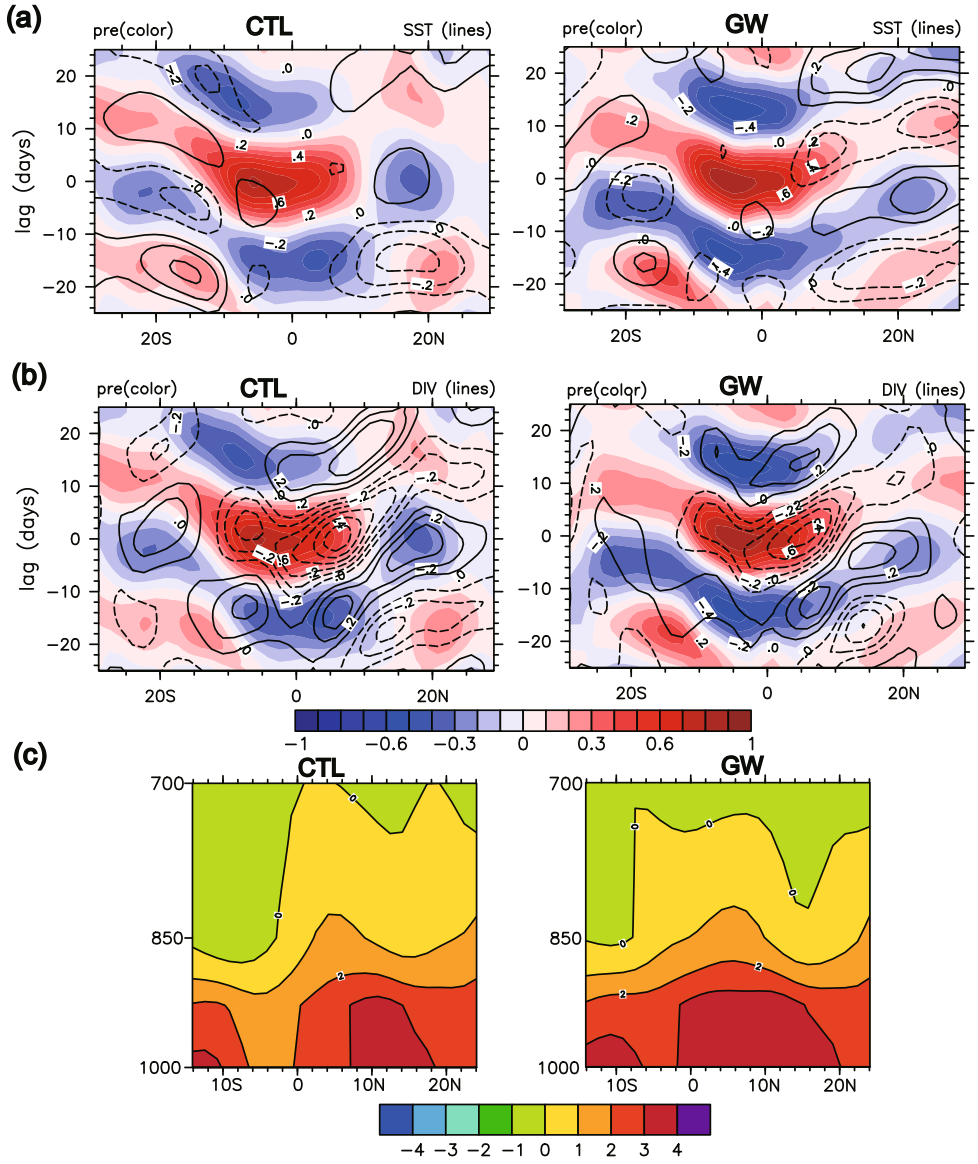

Fig. 3. Lagged-time–latitude diagram of correlation coefficients between 20–100-day band-pass filtered precipitation (color shadings) and (a) SST & (b) divergence (contours) over 75°–100°E during boreal summer against to the 20–100-day filtered precipitation over the reference region (5°N–10°S and 75°–100°E), respectively for CTL and GW runs. (c) Meridional–vertical profile of the north–south component of the summer mean flow (m s^{-1}) averaged between 70° and 95°E, respectively for CTL and GW runs.

the RCP8.5 simulation (Fig. 4c), the eastward propagations of both lower-level wind and rainfall obtain was significantly enhanced from 60°E across the western Pacific to the central Pacific, and the quadrature relationship between precipitation and U850 was stronger.

Next, we analyzed the eastward propagation that markedly intensified in RCP8.5. The eastward propagation of MJO/TISO is a convection-wind coupling process (Zhang, 2005). That is, when the MJO/TISO moves eastward, its convective center (rainfall center here) is more likely to be located between the lower-level westerlies to the west and easterlies to the east (see Madden and Julian, 1972). The enhanced quadrature relationship between precipitation and U850 indicates the intensified convection-wind coupling process (e.g., Madden and Julian, 1972; Hendon and Salby, 1994; Sperber, 2003; Wang, 2005), which facilitated the eastward propagation of TISO. We further examined the differences of the associated equatorial waves between the CTL and the RCP8.5 simulation using a

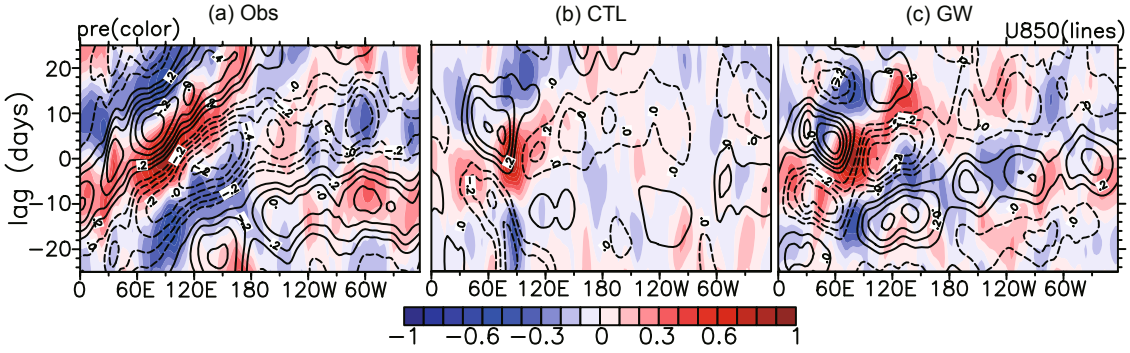

Fig. 4. Lagged-time–longitude diagram of correlation coefficients between 20–100-day band-pass filtered precipitation (color shadings) and U850 (contours) over 10°S–10°N during boreal winter against to 20–100-day filtered precipitation over the reference region (5°N–10°S and 75°–100°E), respectively for (a) observation, (b) CTL simulation, and (c) GW simulation. Contour interval is 0.1.

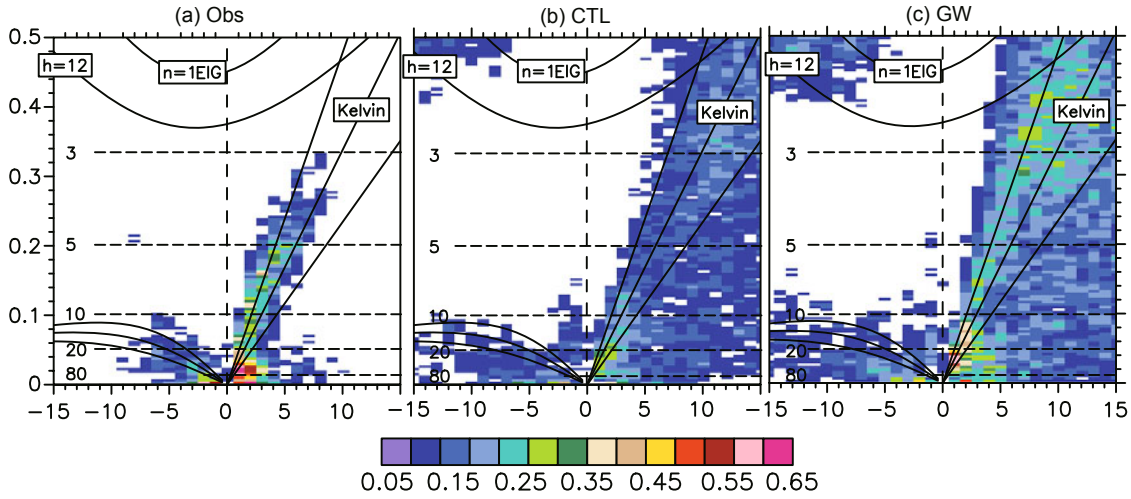

Fig. 5. The symmetric spectrum of coherence squared (color shading) between rainfall and 850 hPa zonal wind, respectively for (a) observation, (b) CTL simulation, and (c) GW simulation. Spectra were computed for individual latitudes, and then averaged over 15°S–15°N. Computations are conducted using data in all seasons on 256-day segments, overlapping by 206 days. Dispersion curves for the Kelvin, equatorial Rossby (ER), and intertio-gravity (EIG) modes.

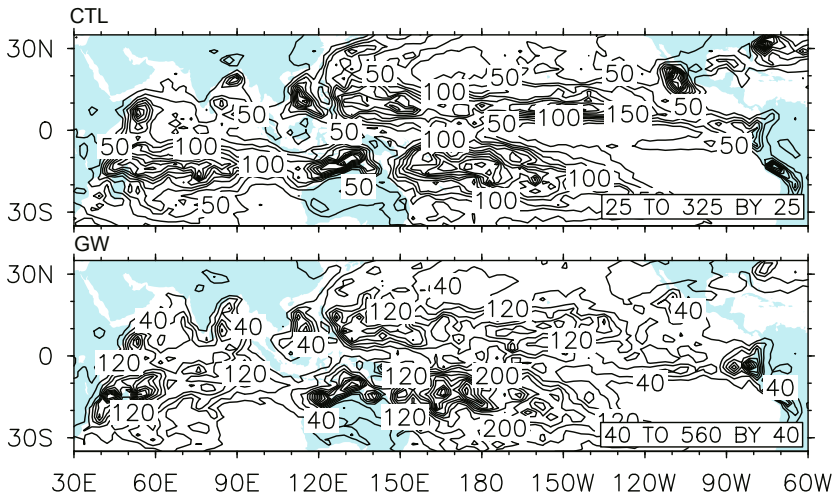

Fig. 6. 20–100 day precipitation variance during Nov.–Apr. period, respectively in historical control simulation and global warming simulation. The units of precipitation variance are $mm^2\ d^{-2}$.

wavenumber–frequency spectra analysis (Wheeler and Kiladis, 1999). Our result shows that the equatorial Kelvin wave in the MJO band, which propagates eastward (Wang, 2002), was remarkably intensified in RCP8.5 (Fig. 5). The enhanced equatorial Kelvin wave corresponded to the intensified eastward propagation. Both the enhanced equatorial Kelvin wave and the intensified convective-wind coupling can be attributed to the warmer SST mean state (Fig. 1), which tended to induce stronger intraseasonal heating response (Fig. 6) and the associated stronger atmospheric response to the heating, particularly over the equatorial Pacific.

5. Conclusion

Using numerical simulations based on the IPCC AR5 scenario, this study investigated the changes in TISO propagation modified by global warming. Compared to the historical simulation CTL, both the northward propagation during boreal summer and the eastward propagation during boreal winter were intensified under the global warming simulation, RCP8.5. Their intensifications were both related to the changes of mean state after global warming. First, TISO intensified northward propagation over the Indian Ocean during boreal summer in RCP8.5, which can be attributed to the enhanced atmosphere–ocean interaction and the strengthened low-level southerly wind of the mean state. The enhanced summer mean southerly wind may have shifted the moisture center north of the TISO convection center, causing northward movement of the convection. Secondly, TISO (MJO) during winter showed enhanced eastward propagation from IO to central Pacific under RCP8.5, and the enhanced eastward propagation is associated with the strengthened convection-wind coupling and intensified eastward equatorial Kelvin wave under a global warming scenario.

TISO/MJO is a complicated issue for atmospheric study, in both observation and simulation. This study only investigated the TISO/MJO projection of one aspect with one model. In future studies, we need to verify the current result with multi-model results of IPCC AR5, additional studies need to be developed to examine likely modifications in amplitude, structure, and evolution associated with TISO/MJO events under global warming.

Acknowledgements. This study was supported by the "973" projects (Grant Nos. 2012CB417203, 2012CB 955400, and 2013CB955803) and "863" project (Grant No. 2010AA012305), and NSFC (Grant Nos. 41005036 and 41023002).

REFERENCES

Annamalai, H., and J. M. Slingo, 2001: Active/break cycles: Diagnosis of the intraseasonal variability of the Asian Summer Monsoon. *Climate Dyn.*, **18**, 85–102.

Bao, Q., and Coauthors, 2010: An introduction to the coupled model FGOALS1.1-s and its performance in East Asia. *Adv. Atmos. Sci.*, **27**, 1131–1142, doi: 10.1007/s00376-010-9177-1.

Bergman, J. W., H. H. Hendon, and K. M. Weickmann, 2001: Intraseasonal air-sea interactions at the onset of El Niño. *J. Climate*, **14**, 1702–1719.

Bond, N. A., and G. A. Vecchi, 2003: The influence of the Madden-Julian oscillation on precipitation in Oregon and Washington. *Wea. Forecasting*, **18**, 600–613.

Ding, Q. H., and B. Wang, 2009: Predicting extreme phases of the Indian summer monsoon. *J. Climate*, **22**, 346–363.

Duchon, C., 1979: Lanczos filtering in one and two dimensions. *J. Appl. Meteor.,* **18**, 1016–1022.

Fu, X., and B. Wang, 2004: Different solutions of intraseasonal oscillation exist in atmosphere ocean coupled model and atmosphere-only model. *J. Climate*, **17**, 1263–1271.

Hendon, H. H., and M. L. Salby, 1994: The life cycle of the Madden-Julian Oscillation. *J. Atmos. Sci.* **51**, 2225–2237.

Huffman, G. J., and Coauthors, 2001: Global precipitation at one-degree daily resolution from multisatellite observations. *J. Hydrometeorology*, **2**, 36–50.

Jiang, X., T. Li, and B. Wang, 2004: Structures and mechanisms of the northward propagating boreal summer intraseasonal oscillation. *J. Climate*, **17**, 1022–1039

Jones, C., and L. V. Caralho, 2011: Will global warming modify the activity of the Madden-Julian Oscillation. *Quart. J. Roy. Meteor. Soc.*, **137**, 544–552.

Jones, C., D. E. Waliser, K. M. Lau, and W. Stern, 2004: Global occurrences of extreme precipitation and the Madden-Julian oscillation: Observations and predictability. *J. Climate*, **17**, 4575–4589.

Joseph, S., A. K. Sahel, and B. N. Goswami 2008: Eastward propagation of MJO during boreal summer and Indian monsoon droughts. *Climate Dyn.*, **32**, 1139–1153.

Kalnay, E., and Coauthors, 1996: The NCEP/NCAR 40-year reanalysis project. *Bull. Amer. Meteor. Soc.*, **77**, 437–471.

Kessler, W. S., and R. Kleeman, 2000: Rectification of the Madden-Julian Oscillation into the ENSO cycle. *J. Climate*, **13**, 3560–3575.

Kiehl, J. T., and P. R. Gent, 2004: The Community Climate System Model, Version 2. *J. Climate*, **17**, 3666–3682.

Kim, D., and Coauthors, 2009: Application of MJO simulation diagnostics to climate models. *J. Climate,* **22**, 6413–6436.

Krishnamurti, T. N., and D. Subrahmanyam, 1982: The 30–50-day mode at 850 mb during MONEX. *J. At-*

mos. Sci., **39**, 2088–2095.

Liebmann, B., and D. L. Hartmann, 1984: An observational study of tropical–midlatitude interaction on intraseasonal time scales during winter. *J. Atmos. Sci.*, **41**, 3333–3350.

Lin, J. L., and Coauthors, 2006: Tropical intraseasonal variability in 14 IPCC AR4 climate models. Part I: Convective signals. *J. Climate*, **19**, 2665–269.

Liu, H. L., and Coauthors, 2004: An eddy-permitting oceanic general circulation model and its preliminary evaluations. *Adv. Atmos. Sci.*, **21**, 675–690.

Madden, R. A., and P. R. Julian 1971: Detection of a 40–50 day oscillation in the zonal wind in the tropical Pacific. J. *Atmos. Sci.,* **28**, 702–708.

Madden, R. A., and P. R. Julian, 1972: Description of global-scale circulation cells in the tropics with a 40–50 day period. *J. Atmos. Sci.*, **29**, 1109–1123.

Madden, R. A., and P. R. Julian, 1994: Observations of the 40–50 day tropical oscillation: A review. *Mon. Wea. Rev.*, **112**, 814–837.

Matthews, A. J., 2000: Propagation mechanisms for the Madden-Julian Oscillation. *Quart. J. Roy. Meteor. Soc.*, **126**, 2637–2651.

Milliff, R. F., and R. A. Madden, 1996: The existence and vertical structure of fast, eastward-moving disturbances in the equatorial troposphere. *J. Atmos. Sci.*, **53**, 586–597.

Moss, R. H., and Coauthors, 2010: The next generation of scenarios for climate change research and assessment. *Nature,* **463**, 747–756.

Pan, L. L., and T. Li, 2008: Interactions between the tropical ISO and midlatitude low-frequency flow. *Climate Dyn.*, **31**, 375–388.

Rayner, N. A., and Coauthors, 2003: Global analyses of SST, sea ice and night marine air temperature since the late nineteenth century. *J. Geophys. Res.*, **108**, doi: 10.1029/2002JD002670.

Rajeevan, M, S. Gadgil, and J. Bhate, 2010: Active and break spells of the Indian summer monsoon. *Proceedings of the Indian Academy of Sciences—Earth & Planetary Sciences,* **119**, 229–247.

Sperber, K. R., 2003: Propagation and the vertical structure of the Madden-Julian Oscillation. *Mon. Wea. Rev.,* **131**, 3018–3037.

Takayabu, Y. N., and Coauthors, 1999: Abrupt termination of the 1997–98 El Niño in response to a Madden-Julian oscillation. *Nature,* **402**, 279–282.

Taylor, K. E., R. J. Stouffer, and G. A. Meehl, cited 2009: A summary of the CMIP5 experiment design. [Available online at http://cmip-pcmdi.llnl.gov/cmip5/experiment_design.html.]

Tian, B. J., and Coauthors, 2008: Does the Madden-Julian oscillation influence aerosol variability? *J. Geophys. Res.*, **113**, D12215, doi: 10.1029/2007JD009372.

Waliser, D. E., K. M. Lau, and J.-H. Kim, 1999: The influence of coupled sea surface temperatures on the Madden–Julian oscillation: A model perturbation experiment. *J. Atmos. Sci.*, **56**, 333–358.

Waliser, D. E., R. Murtugudde, P. Strutton, and J. L. Li, 2005: Subseasonal organization of ocean chlorophyll: Prospects for prediction based on the Madden-Julian Oscillation. *Geophys. Res. Lett.*, **3**, L23602, doi: 10.1029/2005GL024300.

Waliser, D. E., and Coauthors, 2009: MJO simulation diagnostics. *J. Climate*, **22**, 3006–3030.

Wang, B., 2002: Kelvin wave. *Encyclopedia of Atmospheric Sciences*, Holton et al., Eds., Elsevier, Amsterdam, 1062–1068.

Wang, B., 2005: Theories. *Intraseasonal Variability of the Atmosphere-Ocean Climate System*, K. M. Lau and D. E. Waliser, Eds., Springer-Verlag, Heidelberg, Germany, 307–351.

Wang, B., and H. Rui, 1990: Synoptic climatology of transient tropical intraseasonal convection anomalies: 1975–1985. *Meteor. Atmos. Phys.*, **44**, 43–61.

Wang, B., and X. Xie, 1998: Coupled modes of the warm pool climate system. Part I: The role of air-sea interaction in maintaining Madden-Julian Oscillation. *J. Climate,* **11**, 2116–2135.

Weickmann, K. M., G. R. Lussky, and J. E. Kutzbach, 1985: Intraseasonal (30–60 day) fluctuations of outgoing longwave radiation and 250 mb stream function during northern winter. *Mon. Wea. Rev.*, **113**, 941–961.

Wentz, F. J., and Coauthors, 2000: Satellite measurements of sea surface temperature through clouds. *Science*, **288**, 847–850.

Wheeler, M. C., and G. N. Kiladis, 1999: Convectively coupled equatorial waves: Analysis of clouds and temperature in the wavenumber–frequency domain. *J. Atmos. Sci.*, **56**, 374–399.

Wu, G. X., H. Liu, Y. Zhao, and W. P. Li, 1996: A nine-layer atmospheric general circulation model and its performance. *Adv. Atmos. Sci.*, **13**, 1–18.

Yang, J., B. Wang, and B. Wang, 2008: Anticorrelated intensity change of the quasi-biweekly and 30–50 day oscillations over the South China Sea. *Geophys. Res. Lett.*, doi: 10.1029/2008GL034449.

Yang, J., Q. Bao, X. C. Wang, and T. J. Zhou, 2011: The tropical intraseasonal oscillation in SAMIL coupled and uncoupled general circulation models. *Adv. Atmos. Sci.*, **29**(3), doi: 10.1007/s00376-011-1087-3.

Yasunari, T., 1979: Cloudiness fluctuations associated with the northern hemisphere summer monsoon. *J. Metor. Soc. Japan*, **57**, 227–242.

Zhang, Z. D., 2005: Madden-Julian Oscillation. *Rev. Geophys.*, **43**, doi: 10.1029/2004RG000158.